Journal of Structural Geology 31 (2009) 1540–1555

Contents lists available at ScienceDirect

Journal of Structural Geology

journal homepage: www.elsevier.com/locate/jsg

Geometry of an oblique thrust fault zone in a deepwater fold belt from 3D seismic data

Chris Morley [a,b,*]

[a] Baan Yosawaadi, Soi Ari, Phahonyohothin, Bangkok, Thailand
[b] Department of Petroleum Geoscience, Universiti Brunei Darussalam, Tunku Link, Bandar Seri Begawan, Brunei Darussalam 10900, Thailand

ARTICLE INFO

Article history:
Received 29 June 2008
Received in revised form
23 August 2009
Accepted 30 August 2009
Available online 17 September 2009

Keywords:
Deepwater
Thrust
Oblique fault
Fold
Normal fault

ABSTRACT

Growth of a 12 km long, deepwater anticline during the late Pliocene–Recent is documented from 3D seismic reflection data across NW Borneo. The fold is part of a train of folds formed along the slope at the distal margin of the Baram Delta Province. Growth of the anticline involved fold lateral propagation and linkage of two thrusts formed in the anticline forelimb as either break thrusts or as imbricates ramping up from a master detachment (at ~3 km depth). For the southwestern anticline, the northern tip of the NE–SW striking, SE-dipping thrust passes into an E–W striking oblique termination, which lies in the linkage zone between the two anticlines. The thrust termination is characterised by the following changes passing east towards the fault tip: 1) the fault zone dips steeply to the south, then 2) passes to a vertical segment (inferred to have oblique motion), and 3) furthest east the fault dips northwards with an extensional component of displacement. The fault zone terminates in a transtensional graben. This graben does not fit with a simple pull-apart geometry or simple oblique ramp geometry. In the future if the thrust faults propagate together and link this oblique fault zone may develop into an oblique ramp that acts as a transfer zone between the faults. However at present the oblique fault zone appears to be a region of 3D strain, where deformation at the fault tip, and the gravity effects of plunging folds have affected the shallow, weak sediments and given rise to a complex thrust termination at a early stage of thrust and fold development. The oblique structure may have developed in response to strains imposed by the encroachment of the fold and thrust belt on an uplifted basement or volcanic high that forms a pronounced topographic feature across a narrow part of the thrust front, 14 km NW of the most external (oceanward) fold.

1. Introduction

Lateral and oblique ramps in thrust faults are a common feature of compressional belts (e.g. Rich, 1934; Dahlstrom, 1970; Goldburg, 1984; Couzens and Dunne, 1994; Castonguay and Price, 1995; Apotria, 1995; Holl and Anastasio, 1995; Fermor, 1999; Rowan and Linares, 2000; Soto et al., 2002). However, the range of natural possible oblique ramp or other oblique fault geometries in three dimensions is poorly known (Wilkerson et al., 2002). To properly image oblique structures requires 3D seismic data, which is only rarely acquired in typical onshore fold and thrust belts. Consequently the geometries of lateral and oblique structures in thrust belts are known in most detail from analogue modelling (e.g. Apotria et al., 1992; Wilkerson et al., 1992; Dubey, 1997; Schreurs et al., 2002; Soto et al., 2002). This paper describes an example of an oblique fault system associated with an anticline (IX) in a deepwater fold and thrust belt from offshore Brunei Darussalam (Figs. 1 and 2).

2. Geological background and tectonic history

The NW margin of Borneo has been extensively explored for hydrocarbons, and as a result the shelf and upper slope areas of Brunei, Sabah and Sarawak are well known from drilling and seismic reflection data. Several books summarising the data have been published (James, 1984; Sandal, 1996; Petronas, 1999). Prior to the Miocene northern Borneo was largely submerged, and is thought to have occupied a position in the upper plate of a subduction zone, whose associated accretionary prism is represented by the folded and thrusted deepwater Rajang and Crocker Formations that outcrop in NW Borneo (Figs. 3 and 4; James, 1984; Lambiase et al., 2007). The proto-South China Seas oceanic crust is thought to have formed the lower plate, which was subducted to the SE beneath Borneo (e.g. Hazebroek and Tan, 1993; Hall, 2002).

* Tel.: +66 02 538 4624.
E-mail address: chrissmorley@gmail.com

0191-8141/$ – see front matter © 2009 Elsevier Ltd. All rights reserved.
doi:10.1016/j.jsg.2009.08.015

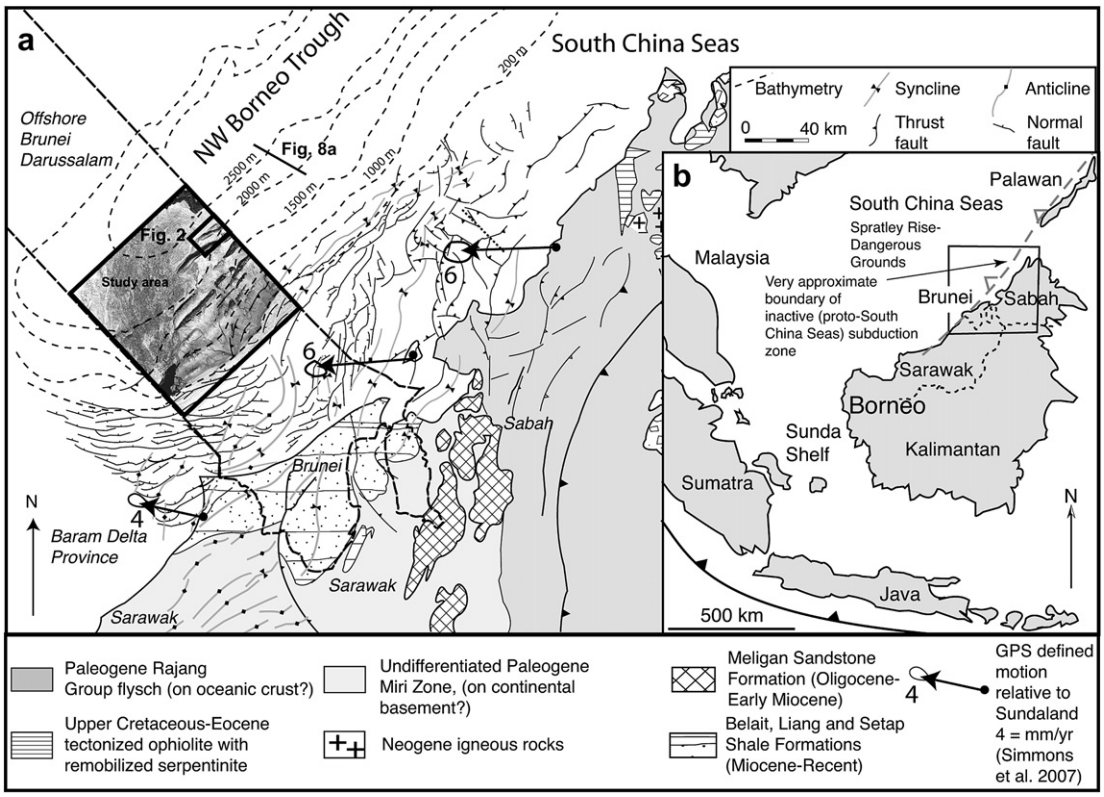

Fig. 1. a) Map of NW Borneo showing location of the NW Borneo trough and study area, offshore Brunei Darussalam. b) SE Asia location map. Modified from Morley and Back (2008).

The deepwater sequences were uplifted during the Miocene, when the relatively buoyant, thinned continental crust of the Dangerous Grounds Crust entered and jammed the subduction zone (e.g. Levell, 1987; Hutchison et al., 2000). Consequently Borneo became uplifted and eroded, and shed huge quantities of sediment onto the margin of the island during the Miocene–Holocene (Hall and Nichols, 2002; Morley and Back, 2008). As a result of uplift and high rates of sediment supply, the Miocene–Holocene shelf of NW Borneo in general, and Brunei in particular is dominated by prograding shallow marine sequences of Middle Miocene–Recent age, which in places attain thicknesses in excess of 10 km. The Miocene–Holocene depocentre in Brunei is known as the Baram Deltaic Province; it is deformed by growth faults, shale diapirs, folds, thrusts and inversion-related anticlines (Morley et al., 2003, 2008). Gravity-driven deformation has occurred by rapid progradation of sand and shale dominated deltaic sequences comprising the Belait and Liang Formations, over a thick marine shale sequence (Setap Formation; Fig. 3). The Setap Formation is composed of overpressured, mobile shales that have flowed and deformed in response to sediment loading by the Belait and Liang Formations.

The general structural evolution of the delta is marked by progradation of growth faults from the onshore area during the Middle Miocene, towards the offshore with time. At the present day, the most active growth faulting occurs around the outer shelf-uppermost slope (Figs. 4 and 5). The Baram Deltaic Province is not a classic passive margin delta because it has been subject to thrusting, folding and inversion of growth faults in the proximal part of the province from the late Middle Miocene to the early Pliocene (Sandal, 1996; Morley et al., 2003, 2008; Figs. 4 and 5).

At the offshore (distal) end of the deltaic province is another fold and thrust province located on the slope in the deepwater equivalents of the extensively drilled Baram Delta Province Middle Miocene–Recent shelfal sequences (Fig. 4). The slope dips between one and three degrees into the deepest region of the South China Seas: the Northwest Borneo trough. 2D seismic data have shown the NW Borneo trough marks the site of inactive subduction where thinned continental crust of the Dangerous Grounds block entered the subduction zone (Levell, 1987; Hall, 1996). The existence of the fold-thrust belt has been established by sparse industrial and academic 2D seismic lines (James, 1984; Hinz and Schluter, 1985; Hinz et al., 1989; Sandal, 1996; Schluter et al., 1996; Pin and Hailing, 2004). The 2D seismic data shows an extensive train of folds spaced between 5 and 15 km apart affects the slope, and generally verge offshore. They are predominantly folds associated with imbricate thrusts that sole out at depth into one or more detachments (e.g. Franke et al., 2008; Hesse et al., 2008). The thrust belt has a classic taper geometry, with the basal decollement dipping shelfward. At the shelf-slope break the detachment probably lies at a subseafloor depth of about 10 km, while at the thrust front the depth is about 3 km (Morley, 2007a).

The present-day fold-thrust belt is largely of latest Miocene–Recent age (Sandal, 1996; Ingram et al., 2004). Deformation is unrelated to past subduction of oceanic crust. The active folds trend NE–SW, parallel to the old subduction zone and the ancient subduction zone appears to have continued to act as a major zone of weakness in the crust (Hall and Morley, 2004). GPS data shows that northern Borneo is moving west at about 4–6 mm/yr with respect to Sundaland (i.e. Palawan, South Borneo, Peninsula Malaysia and Indochina; Simmons et al., 2007)). This motion is oblique to the NE–SW striking folds of the continental slope and oblique to the modern maximum horizontal stress direction (NW–SE) determined for the shelf immediately adjacent to the GPS points (Tingay et al., 2005; King et al., 2009). The stress tensor for the deepwater area is a combination of gravity-driven deformation

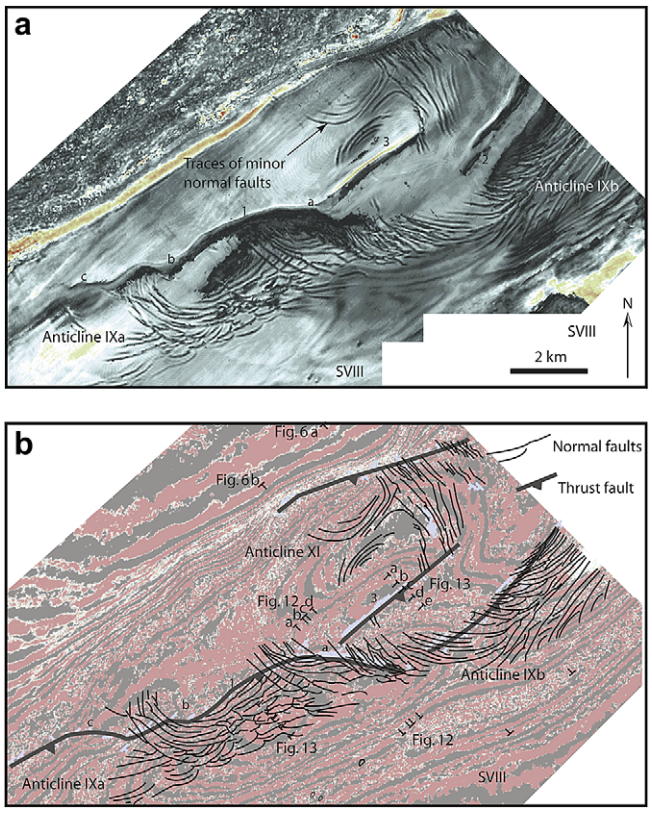

Fig. 2. Maps of anticlines IX and XI illustrating a) the normal fault geometry on an amplitude map of horizon B, and b) the geometries of deeper thrusts and shallower normal faults on a time slice at 3805 s. See Fig. 1 for location. 1, 2 and 3 = thrust faults. a, b and c = location of oblique structures along the thrust faults.

and far-field tectonic stress (e.g. Hall and Morley, 2004; Simmons et al., 2007; Tingay et al., 2005; Morley et al., 2008; Hesse et al., 2008; King et al., 2009). The dual stress system has been established by a number of observations including: 1) inner shelf-onshore inversion of growth faults (Morley et al., 2003, 2008), 2) modern maximum horizontal stress orientations that lie sub-perpendicular to the coastline in the onshore and inner shelf area, and the continental slope, and that only lie sub-parallel to the margin in the zone of active extension around the outer shelf (Tingay et al., 2005; King et al., 2009), and 3) shortening in the deepwater fold and thrust belt that is greater than the amount of extension in the more proximal area of the deltaic province (Hesse et al., 2008; King et al., in press). The gravity-driven component of stress may help explain the difference between the modern stress orientation and GPS-defined block motions. This combination of near-field and far-field driving stresses is a significant difference from deltas on passive margins, such as the Niger Delta and Gulf of Mexico, where near-field gravity stress is the sole driving mechanism.

3. Data and methodology

A 10,000 km^2 marine 3D seismic data set covering the deepwater area of Brunei Darussalam was acquired using 10, 6 km long streamers by PGS in 2000/2001. This paper is part of a study at the University of Brunei Darussalam that utilised the deepwater 3D survey provided by an agreement between the Petroleum Unit, Total and Brunei Shell. The data set used in this study is clipped at one second below the sea floor, to preserve confidentiality for hydrocarbon exploration. This would be approximately equivalent to 0.8–1 km depth of section, of predominantly Pliocene–Recent age.

The base-of-slope anticlines discussed in this paper were mapped as part of a regional project using the 3D seismic data set. For ease of comparison with other publications on the area, the number and letter designations of locations, anticlines and horizons are kept constant. However, this means some labelling is not consecutive, for example the regional horizon A did not extend into the area described in this study, hence there is only reference to horizons B, C and D.

Four horizons were picked in the study area: the water bottom reflection (Fig. 6), the top (horizon B) and bottom (horizon C) of a distinctive low reflectivity package, and the deepest possible horizon (horizon D) that could be mapped around most of the study

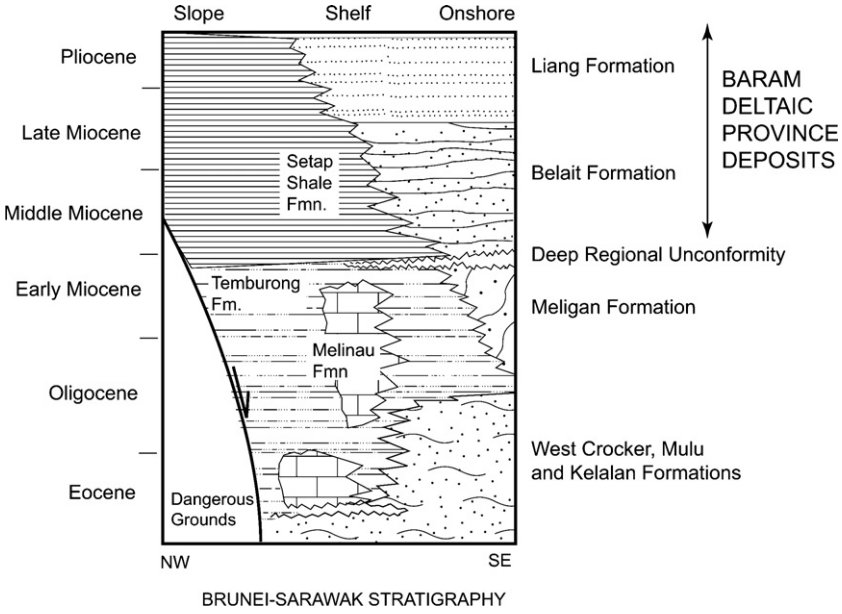

Fig. 3. Regional stratigraphy of NW Borneo, modified from Sandal (1996).

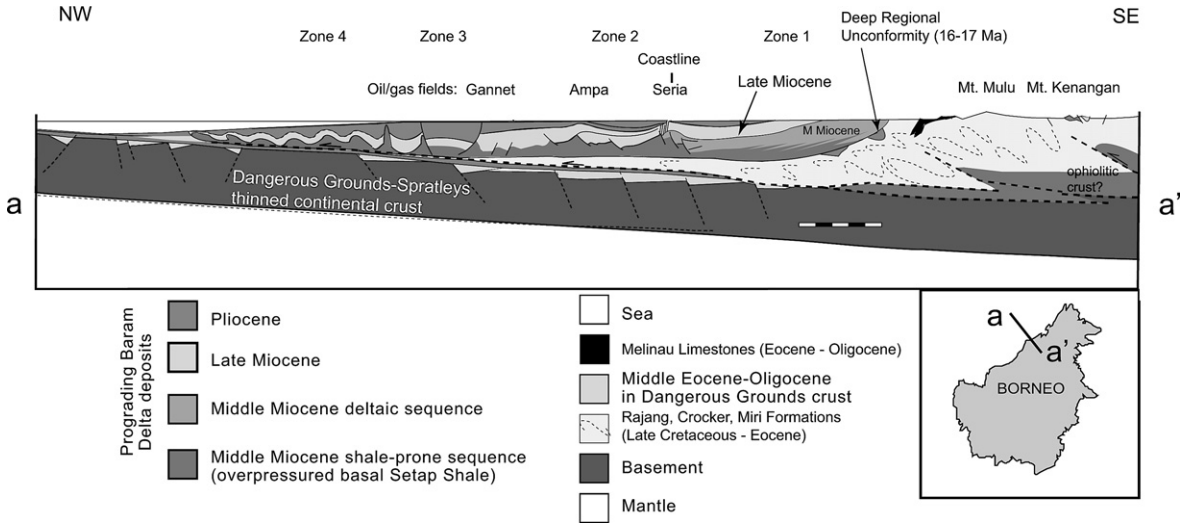

Fig. 4. Regional cross-section illustrating the large-scale structural setting and geometry of the Baram Delta province. Modified from Hall and Morley (2004). The Baram Delta province displays the following structural zones passing from onshore to offshore: 1) Zone 1, N–S trending folds and thrusts. The steeply dipping beds display large-scale progradational geometries in the Belait Formation on satellite images. This zone is not affected by gravity related normal faults or diapirs. 2) Zone 2, mixed growth faults and anticlines. From about 25 km inland to the mid-shelf is a zone of NE–SW striking growth faults, together with N–S and NE–SW striking folds related to episodes of inversion during the Miocene–Pliocene. 3) Zone 3, young growth faults. The outer shelf tends to be dominated by young, offshore dipping (regional) growth faults and some mud pipes. 4) Zone 4, the slope-deepwater fold and thrust belt. Most of the structures above with the likely exception of the N–S striking folds in zone 1, are developed above a basal detachment zone in the Setap Formation.

area. The lower horizons (C and D) tend to lie within lower amplitude, more continuous reflection packages, and regionally lie within sedimentary packages deposited during the early stages of fold development. While some highly discontinuous to chaotic units are present, in general the reflection continuity is good and reflectors tend to be sub-parallel. Horizon B is located near the base of a higher amplitude reflection package that represents the infill of synclinal mini-basins. The mini-basin fill contains a wide range of reflection patterns types, ranging from parallel, continuous reflections, to discontinuous, mounded or wavy forms. Erosional truncations are frequent. Seismic velocities across the upper one second are very slow, between ~1800 and 2000 m/s.

To obtain a high-resolution interpretation across the area, horizons B, C and D were picked every 25 lines and traces. Line spacing is every 12.5 m, hence the spacing of the 25×25 grid is 312.5 m. The final infill of the grid to produce a continuous horizon was conducted using the automatic picking software (Zap) within the interpretation package. The autopicker uses the manually picked grid as the seed points for propagating the grid constrained by seismic attributes and a window of operation. Autopicking works best where the attributes of the event being tracked are constant or change gradually, areas with faulting and complex sedimentary features are not ideal for autopicking, and the manually picked grid must be made finer in such regions. Hence in some areas, particularly those affected by abundant faulting (Fig. 7c), channels, other erosional features and debris flows, lines and traces were picked every 2–10 lines. On vertical sections through the seismic data fault zones tend to show up as narrow zones of weak amplitude. Faults were picked manually on cross-sections, however very good map view images of fault traces could be obtained without picking because the amplitude anomalies associated with faults showed good definition on amplitude maps (Fig. 2a). To determine the sedimentation and fault patterns in map view from amplitude anomalies, two methods were used: 1) the amplitude of the autopicked horizon, and 2) the root mean square (RMS) of anomaly values for a 10 ms window of data sampled above or below a smoothed version of the picked horizon using StratAmp software. For further details of these methods see Brown (1996). Similar results were obtained using the different methods, but the clarity of fault definition varied.

4. Structural setting of the fold deepwater and thrust belt

4.1. Fold geometries at depth

Published seismic sections across the deepwater fold belt in Brunei and Sabah show that most folds are underlain by shelfward-dipping, imbricate thrusts that sole into a deep detachment zone

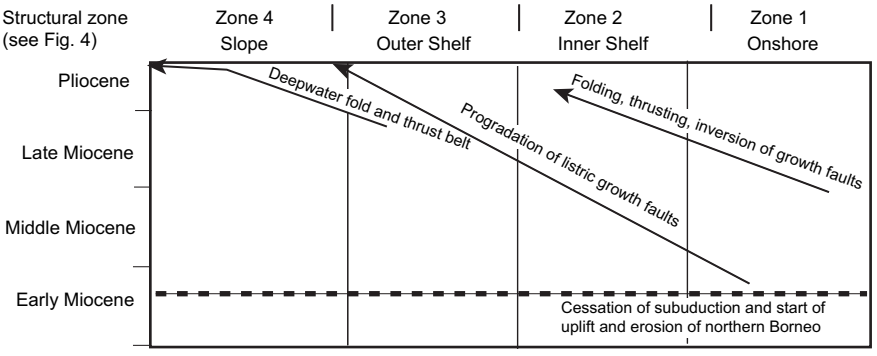

Fig. 5. Chart showing the main timing of structural events vs. position within the delta (see Fig. 4).

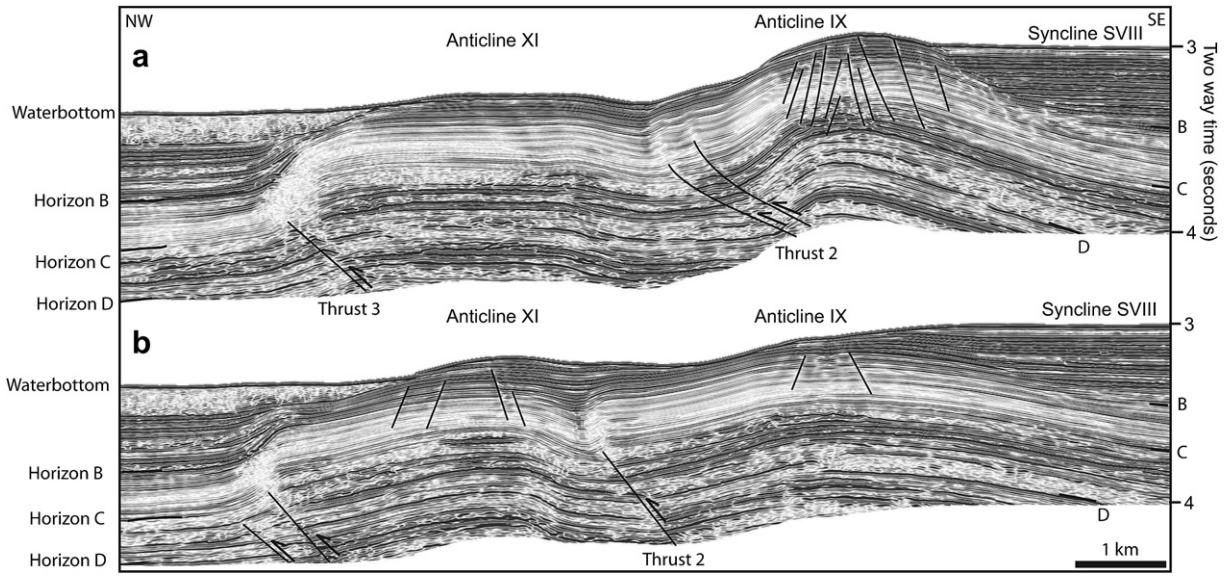

Fig. 6. Seismic lines across the most external or oceanward anticline (IX), showing that the seafloor is folded quasi-conformably with more internal reflections. The anticlines contain crestal normal faults, and developed with propagating blind thrusts present in the lower part of the seismic section. The thickness of the seismic data below the sea floor is 1 s two-way travel time (TWT), which is approximately equal to 0.9 – 1 km thickness of section. See Fig. 2b for location.

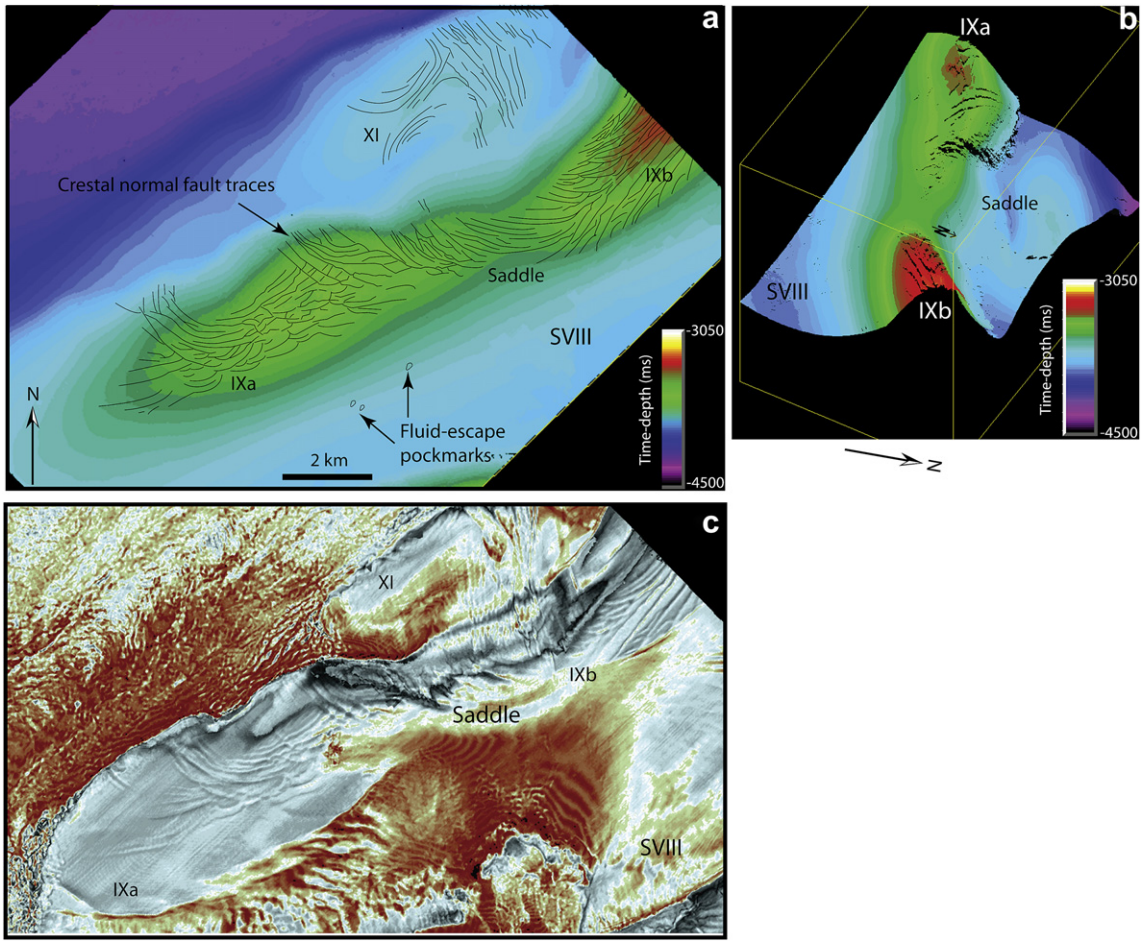

Fig. 7. a) Time structure map for horizon B for anticlines IX and XI with normal fault pattern superimposed, b) 3D perspective view of the time structure map in a) looking to the SW of the time structure map in a), c) RMS amplitude map (10 ms window) of water bottom for anticlines IX and XI shown near-surface fault pattern.

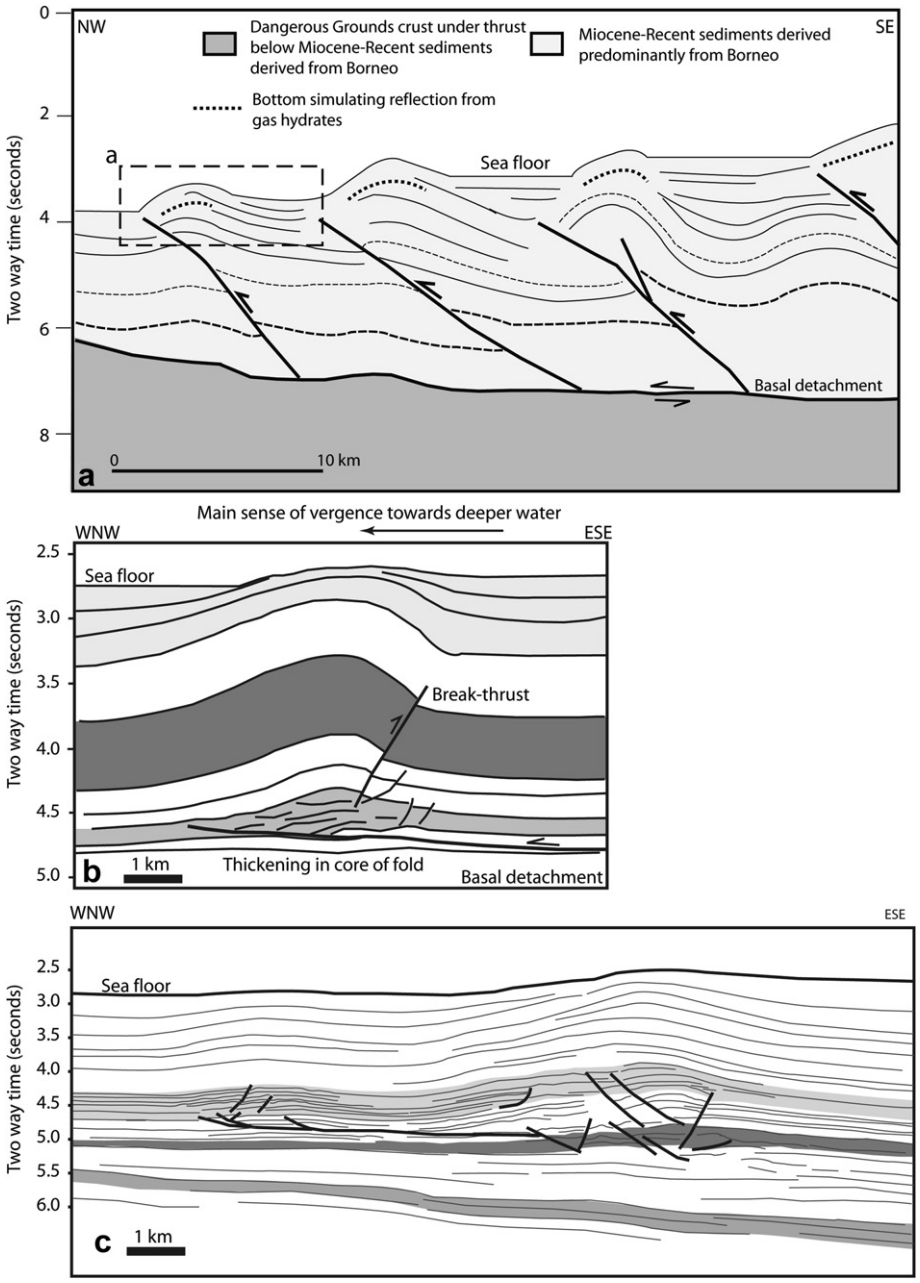

Fig. 8. a) Line drawing of part of regional 2D seismic line in Hinz et al. (1989) across the deepwater fold and thrust belt in Sabah. Box a) shows the approximate equivalent extent of the seismic data used in this study (e.g. Fig. 6). See Fig. 1 for location. b) and c) Line drawings of 2D seismic lines from external deepwater folds of adjacent areas of Borneo illustrating the deep structural geometries associated with the early stages of fold development.

(James, 1984; Sandal, 1996; Ingram et al., 2004). In the deepwater area of NW Borneo, regional 2D seismic reflection data shows that the thrust ramps form a wide variety angles to the dip of the strata in the backlimb (e.g. Ingram et al., 2004; Hesse et al., 2008; Fig. 8a), unlike simple fault-bend fold or fault propagation folds models where the backlimb dips at the same angle as the thrust ramp (e.g. Suppe, 1983; Suppe and Medwedeff, 1984). Some imbricate thrusts display ramp-flat-ramp geometries, which are unlikely to be due to significant changes in competency of the strata, but may reflect fault propagation after folding had begun. The folds have developed in poorly lithified sediments, unsuited for flexural slip-type folds. They do occur in a very similar deepwater setting and display similar geometries (Fig. 5a) to the shear fault-bend folds described by Suppe et al. (2004), which have pre-kinematic backlimb dips that are lower-angle than the underlying thrust ramp (Fig. 8). Deepwater folds associated with the Niger Delta have been interpreted as shear fault-bend folds, which can have simple-shear and pure-shear variations (Corredor et al., 2005; Fig. 9).

In the idealized shear fault-bend folds of Suppe et al. (2004), it is only the hangingwall section that undergoes thickening (Fig. 9). In the deep seismic lines across NW Borneo (Fig. 8a) the forelimb thrusts commonly cut across a footwall syncline, the geometry indicates the anticline developed prior to simple ramp-flat thrust development and that the zone of thickening extends into what later becomes the footwall area (Fig. 8b,c). In some examples of early stage folds, it can be seen that thickening by flow of mobile shale, or movement of numerous small thrusts with multiple local minor detachment levels, and often dual vergence directions in the

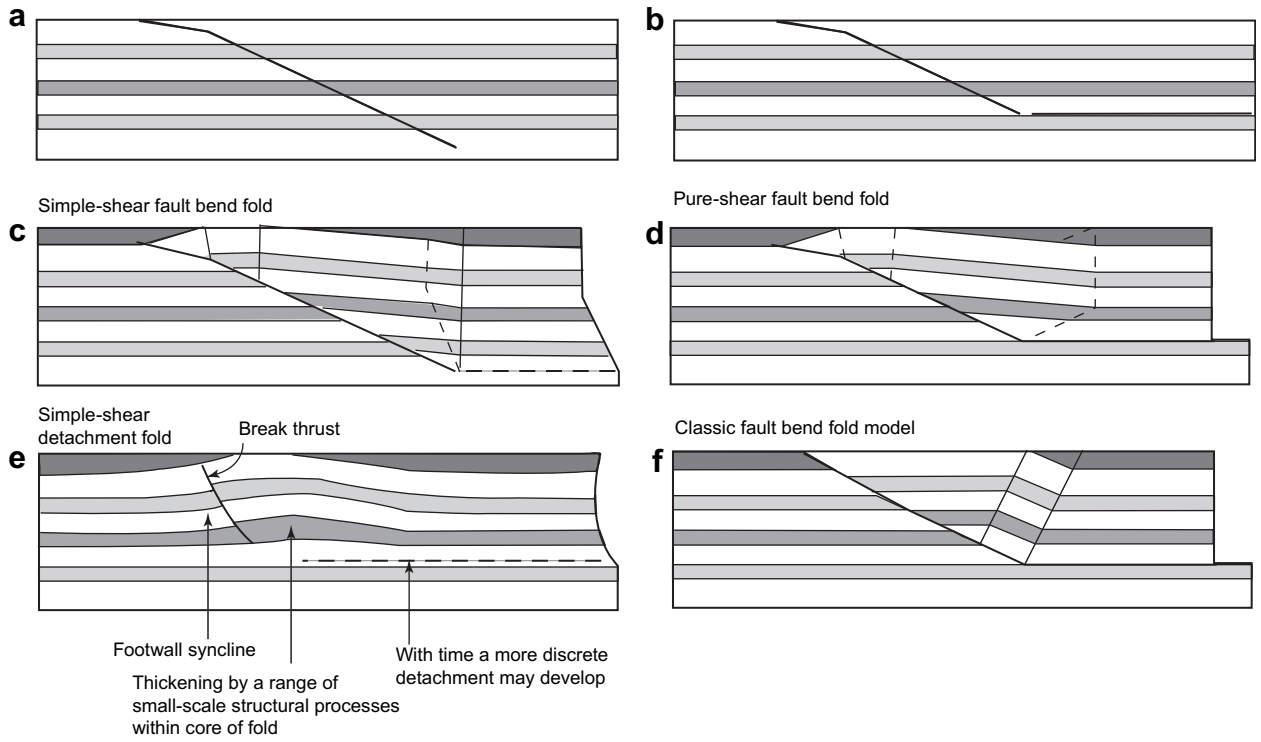

Fig. 9. Forward models from starting points a) and b), of c) simple-shear fault-bend folds, d) pure-shear fault-bend folds, e) simple-shear detachment fold. Simple-shear folds do not require slip along a discrete detachment; a detachment zone undergoes an externally imposed bedding-parallel simple shear, f) Classic fault-bend fold. In pure-shear fault-bend folds, slip occurs along a discrete detachment, and a zone in the hangingwall undergoes shortening and thickening above the fault ramp. In the detachment folding example, heterogeneous shear occurred, with a basal detachment zone (like the simple-shear fault-bend fold), but also layer thickening (like the pure-shear model). The formation of a break thrust after initial folding results in folding and thickening in both the hangingwall and footwall areas of the break thrust. This scenario can explain the geometries seen in Fig. 8b and c. a–e based on Suppe et al. (2004), and Corredor et al. (2005).

anticline core commonly precede establishment of a recognisable simple ramp-flat thrust and can help explain the footwall syncline geometry (Fig. 8b and c). Structurally induced compaction and dewatering may also play a significant role in the early stage of deformation (e.g. Morgan and Karig, 1995; de Vera et al., 2009). In the Orange Basin, the difference between extension (24 km) and shortening (16 km) measured from large-scale structures visible on seismic lines, suggests sub-seismic deformation processes may account for about 24% shortening (de Vera et al., 2009).

The more local thickening by small structures prior to the establishment of large thrusts gives rise to folds preceding the development of thrusts. The folds can subsequently develop thrust faults within the fold limbs that propagate downwards to join the basal detachment (Eisenstadt and De Paor, 1987; Fischer et al., 1992; Morley, 1994; Fig. 8c). Note that in Fig. 8c not only does the thrust in the fold limb die out before reaching the basal detachment, but the vergence of the fold, and the backlimb thrust is opposite to the sense of motion on the detachment. Hence in this case a classic fault bend, fault propagation fold or shear fault-bend fold model is more clearly inappropriate than in many examples. Consequently, at least one mode in which imbricate faults develop in a deepwater setting is in the style of break thrusts (Fischer et al., 1992; Morley, 1994), rather as faults propagating upwards from a major decollement as in the shear fault-bend fold model, as appears to be commonly assumed at present. While the early stage folds can be described as detachment folds, they differ in not necessarily occurring along a discrete detachment. Following application of the term shear fault-bend folds from Suppe et al. (2004), the folds in Fig. 8b, and c can be described as shear detachment folds (Fig. 9e).

4.2. Fold patterns

The deepwater fold belt displays up to ten major anticlines along the slope (Fig. 10). The amount of shortening and the number of folds dies out to the SW. While the anticlines trend sub-parallel to each other, fold axis orientation changes by up to 20°, with the more landwards fold set in the NE half of the area trending NE–SW and the fold set in the SW half of the area trending more ENE–WSW (Fig. 10). The reason for this change in orientation appears to be caused by one or a combination of two features. First, two main deltaic depocentres have been identified: the Baram Delta in the southern part of the area, and the Champion Delta in the northern part of the area (Sandal, 1996; Fig. 10). The change of the fold trends coincides well with the depositional limits of the deltas, and could represent the different directions of loading and delta progradation associated with the two deltas (Fig. 10). The second feature is the geometry of the onshore /inner shelf zone of thrusting and folding, which is oriented more ENE–WSW in the western part of the area and more NE–SW in the eastern part of the area (Fig. 10). These underlying trends, and the greater uplift of the shelf area in the eastern part of the area may have also contributed to the fold geometry of the deepwater area.

5. Geometry of anticline IX

Anticlines IX and XI are the most distal folds in the series of toe thrusts and folds developed on the continental slope offshore Brunei Darussalam. The anticline displays a smooth, convex morphology at the sea floor, largely lacking the landslides and erosional features that affect the more mature anticlines in the area

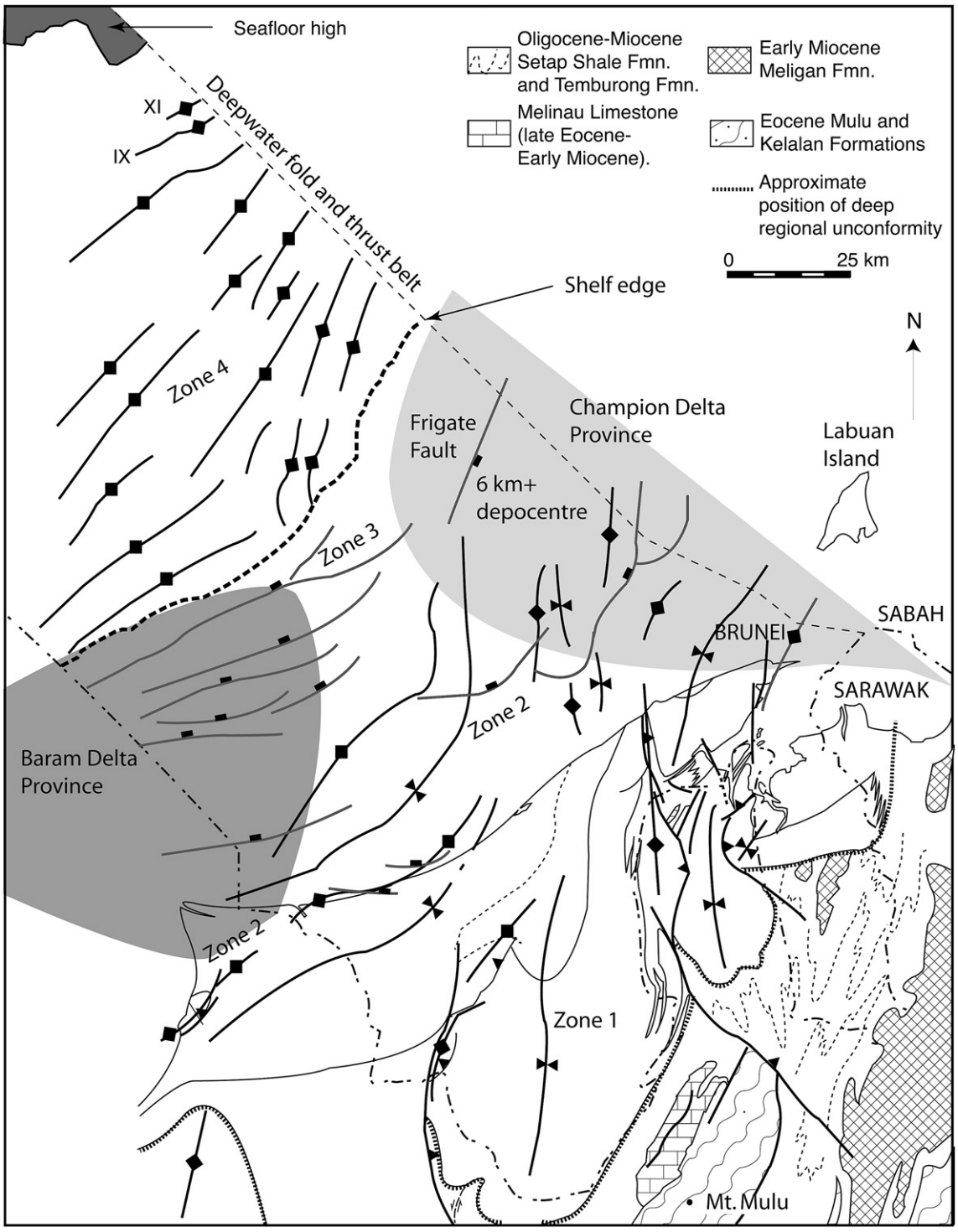

Fig. 10. Regional structural map of onshore and offshore Brunei compiled from data in James (1984), Sandal (1996), Morley et al. (2003), and Morley (2009), also showing anticlines IX and XI, which are the focus of this study.

(Morley, 2007b). The fold morphology, coupled with the large interlimb angle (160°–170°), and late development growth strata patterns post horizon B (Fig. 2) compared with anticlines higher up the slope, all point to the anticline being one of the more recently developed folds in the deepwater area.

In map view anticline IX trends NE–SW, it has two crests (IXa and IXb, Figs. 2 and 7c) that are weakly en echelon, and an intervening low relief saddle area. In the saddle area is the oblique fault trend that is the focus of this paper (Fig. 2 location a). Anticline IXa has a periclinal geometry, the anticline to the SW simply plunges and dies out. To the northeast the anticline plunges into the saddle region and the structure becomes more complex. Not only does the anticline link with anticline IXb, but also a second anticline (XI) is present, the area displays three blind thrusts (locations 1, 2 and 3, Fig. 2). Thrust 1 shows a right-stepping geometry, with oblique trends at locations c, b and a (Fig. 2), of which location a is the

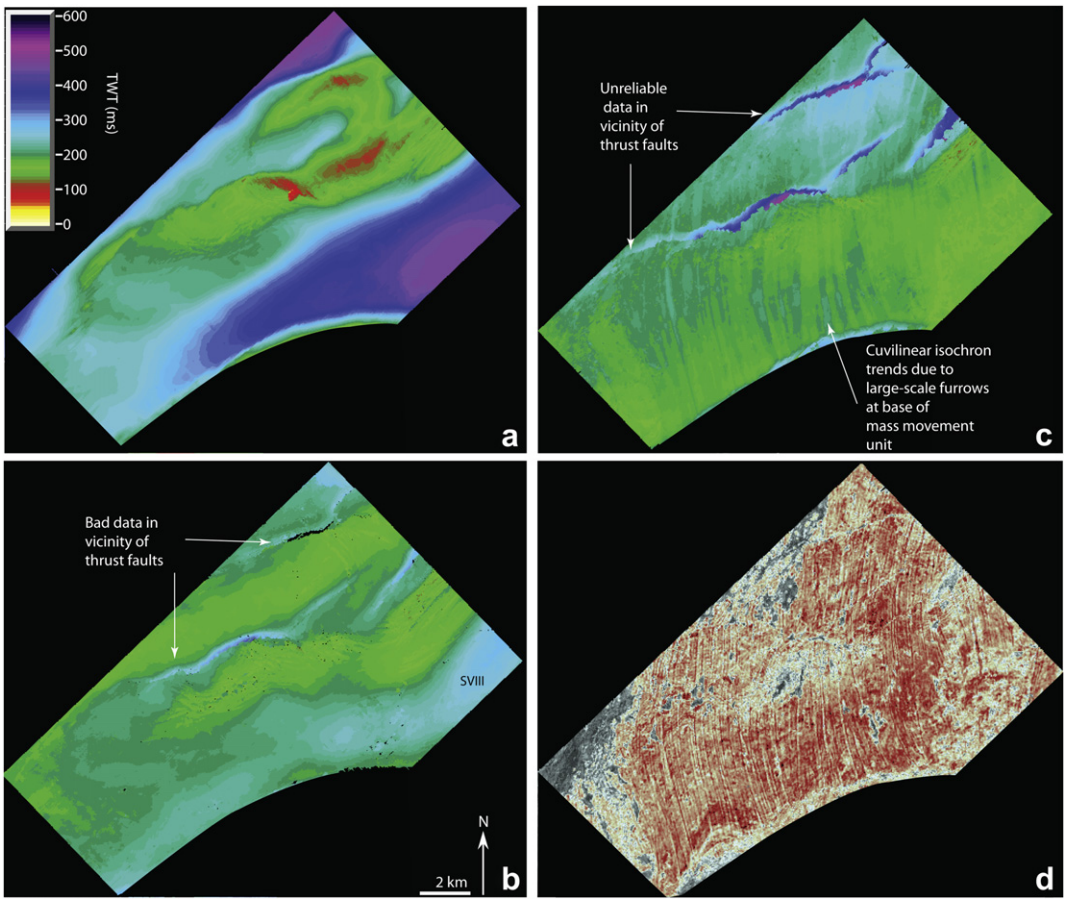

Fig. 11. Isochron maps in milliseconds for interval thickness between mapped horizons. a) Interval horizon B–seafloor, b) horizon C–horizon B, c) horizon C–horizon D, d) amplitude map on horizon D illustrating that the curvi-linear features on the isochron map c, are seen as amplitude anomalies at the base of a mass flow unit. N–S trending furrows at the base of the unit overlying horizon D. In the study area the unit overlying horizon D is transparent and internally chaotic, consequently it is interpreted to be a produce of mass movement, probably a debris flow. The furrows are up to 20 m deep, and 100–400 m wide.

largest. The thrusts dip landward, die out towards the sea floor and lie in the forelimbs of the folds. 2D and 3D seismic data show that the thrusts continue at depth (~3 km sub-sea floor) to join a master detachment (Fig. 5a). As discussed in Section 4.1, the thrusts probably originated as break thrusts (that subsequently linked) during the development of an early stage shear detachment fold.

Crestal normal faults developed in the upper part of the section are a prominent feature of anticline IX (Figs. 2 and 6a). In map view the normal faults swing from a NE–SW direction to a NW–SE strike in the vicinity of lateral ramps a and b (Fig. 2). These changes correspond with oblique surface dips, where the anticline plunges towards the oblique ramps. The crestal normal faults tend to die out within 500 m of the surface.

6. Timing of folding of anticline IX

The timing of fold growth can be determined by the pattern of thickening and thinning of units (in two-way travel time) between mapped horizons (Fig. 11). The most commonly generated maps from seismic data that record thickness variations are isochron maps. These maps which represent the vertical thickness differences in time between two horizons are the time-equivalent of isochore maps. Ideally for structural studies, particularly when strongly inclined strata are present, the time-isopach maps (i.e. interval thickness measured perpendicular to bedding) should be used, but such programs are not present in standard seismic interpretation packages. Care needs to be taken when interpreting isochron maps, but they remain a useful indicator of structural timing and can be cross-checked with geometries seen on vertical seismic lines.

The dip lines in Fig. 12 from a to d step progressively northeastwards across a short segment of anticline IX (see Fig. 2 for location). Between horizons HD and HC there is no significant thickness change, between HC and HB the section thickens NW of the anticline crest, while above HB thinning onto the fold crest is pronounced. These trends are seen across the study area on the isochron maps (Fig. 11), the section between horizons C and D shows no geometry suggestive of thinning onto folds. Instead the isochron geometries are dominated by N–S curvi-linear trends that are associated with striations on amplitude maps (Fig. 11c and d). These striations or furrows are associated with small downward deflections of the mapped seismic peaks amplitude, that when depth converted indicate erosional features at the base of a mass movement unit some 6–20 m deep and 100–400 m wide. Similar features associated with mass wasting have been described Gee et al. (2005, 2007) and Morley and Leong (2008). The furrows traverse the crests of present-day anticlines undeflected suggesting no strong surface topography was present at the time of transport. Hence both the isochron pattern and furrow geometry indicate no anticline development between horizons D and C. The isochron for horizons C and B shows thinning onto the anticline fold crest, but thickness variations between synclinal areas and the anticline crests are small (between 180 and 250 ms; Fig. 11b). The algorithm

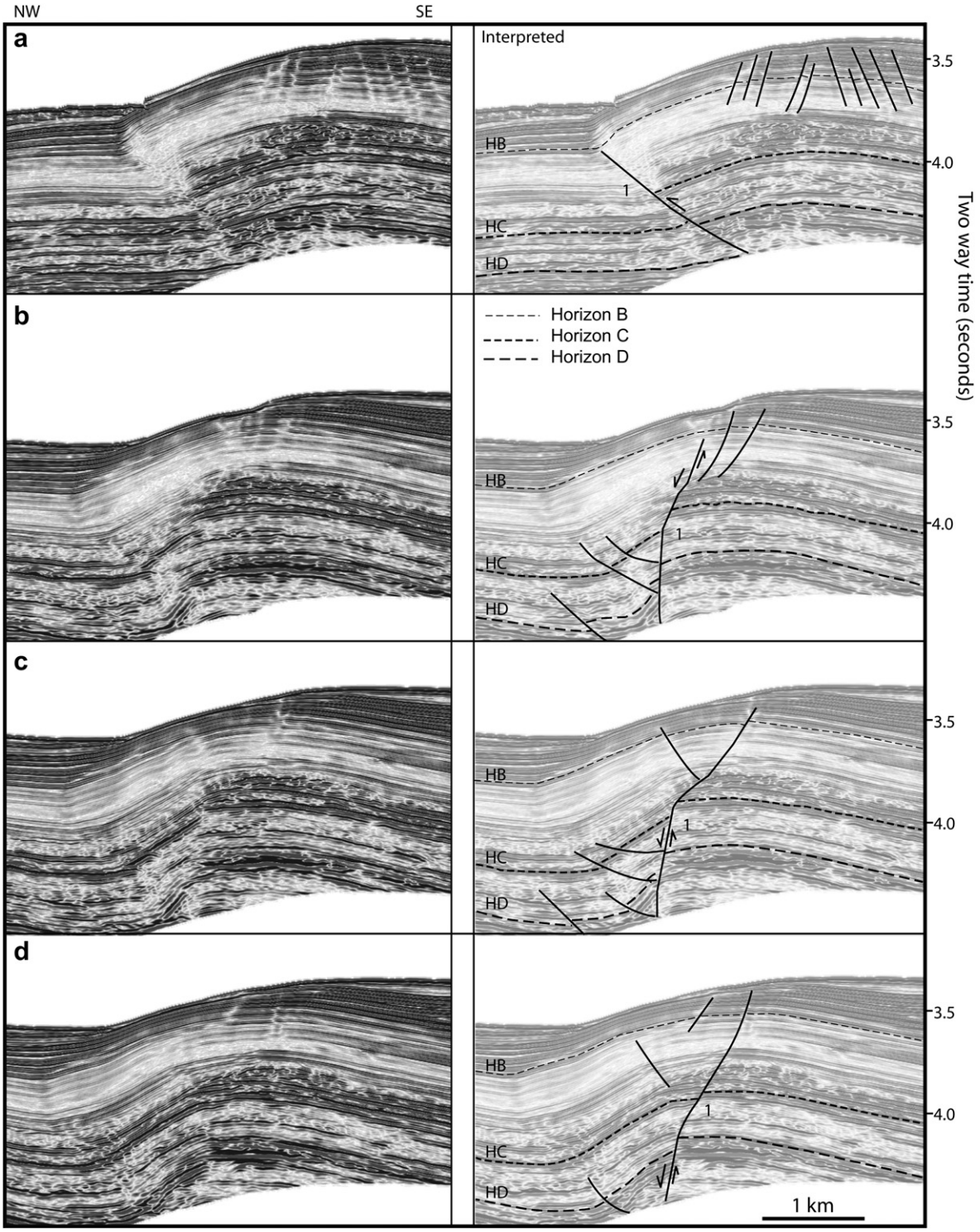

Fig. 12. Dip lines across the oblique fault affecting anticline IX (see Fig. 2b for locations). HB, HC and HD = horizons B, C and D respectively.

that calculates the isochron maps does not cope well with areas where thrusts are present. Consequently a number of the narrow linear trends of increased Isochron thickness between the anticlines are unreliable indicators of fold activity. The isochron for horizon B to the sea floor shows the most significant change in isochron thicknesses, which ranges between about 500 and 80 ms, and clearly indicates the timing of anticline growth (Fig. 11a).

Projection of age dates from wells and seismic reflectors across the shelf and upper slope of the area (data from Sandal, 1996; Ingram et al., 2004) show the upper one second of data in the deepwater area is largely of upper Pliocene to Recent age. Absolute ages for the Late Miocene–Pliocene sequence tied to seismic horizons are provided in Ingram et al. (2004) and are based on a large amount of well data from NW Borneo where dating by micropalaeontology was tied to sea level curves. The character of the reflection packages indicates Horizon D overlies the Lingan Fan II of Ingram et al. (2004) which points to an age of ~3.7–3.5 Ma for horizon D. Regionally mini-basin fill from horizon D or

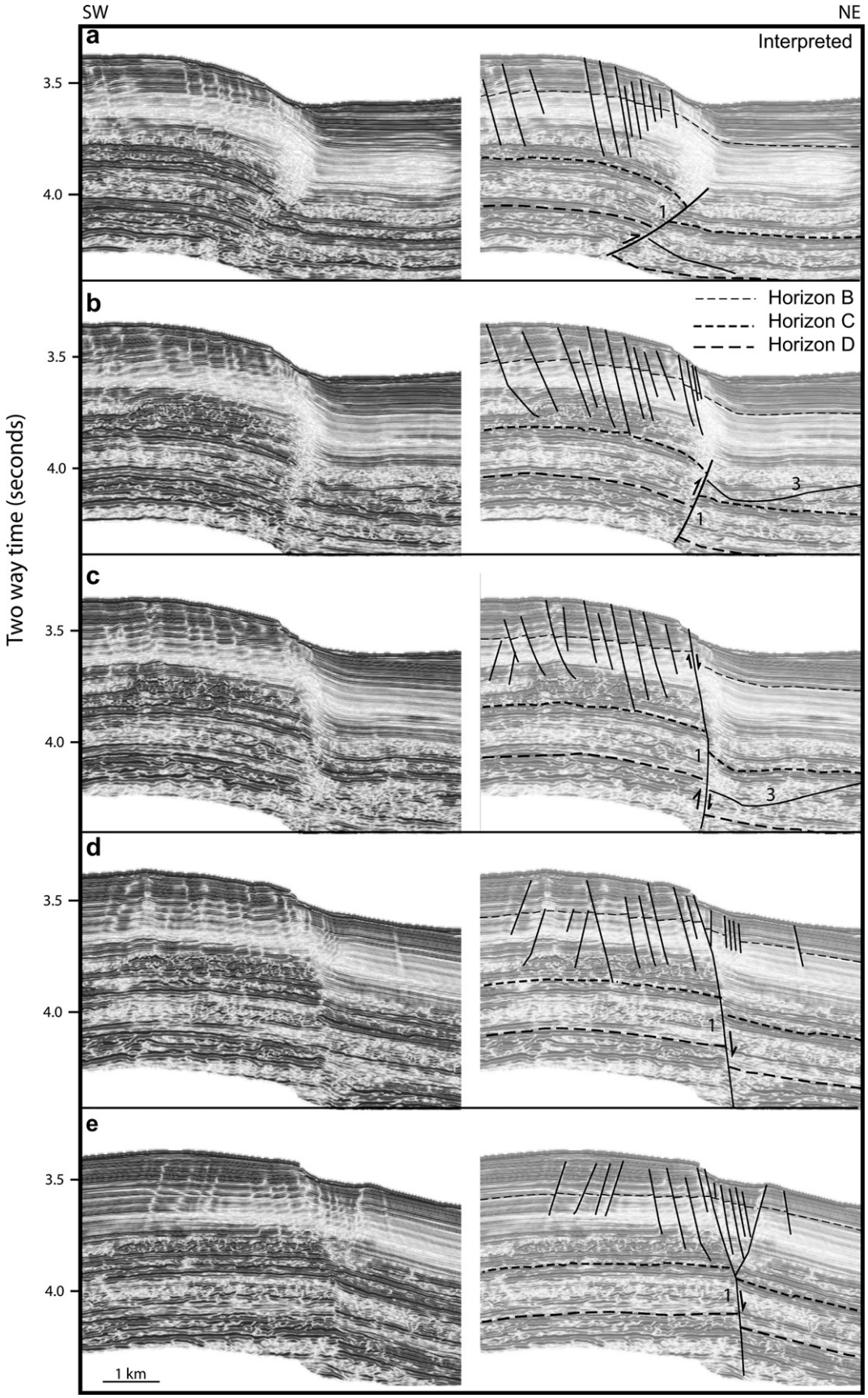

Fig. 13. Strike-lines across the oblique fault affecting anticline IX (see Fig. 2b for locations). HB, HC and HD = horizons B, C and D respectively.

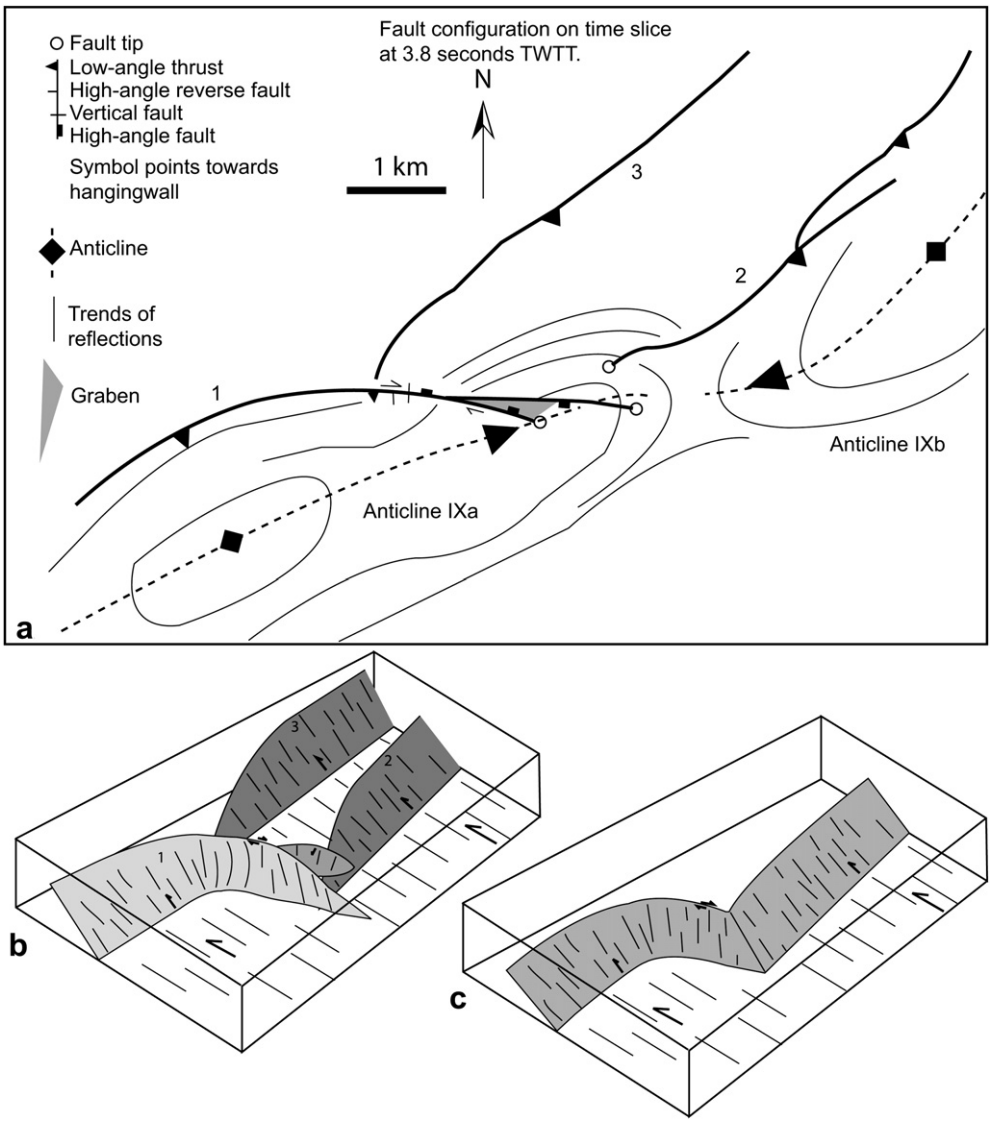

Fig. 14. Oblique fault models: a) structural sketch of anticline IX and the characteristics of fault 1, b) 3D sketch showing characteristics of the thrust and oblique fault segment of fault 1, c) 3D sketch of idealized simple oblique ramp.

C to the sea floor typically ranges from 550 to 900 m, yielding average sedimentation rates of about 0.16–0.25 mm yr^{-1}. For a longer time interval (9 my) the age data provided by well data from adjacent areas yields similar results of 0.28 mm yr^{-1}in a syncline and 0.13 mm yr^{-1}on an anticline crest (Ingram et al., 2004).

For anticline IX growth appears to have begun just below horizon B; the syn-kinematic sediment thickness in mini-basin SVIII is about 450 m (Figs. 11 and 12). Assuming average sedimentation rates between 0.16 and 0.28 mm yr^{-1} for the mini-basin fill, then the age of onset of folding lies between 2.8 Ma and 1.6 Ma (Morley, 2009).

7. Geometry of oblique fault 'a'

The changes in thrust fault geometry around oblique ramp 'a' are illustrated on a series of strike and dip lines (Figs. 12 and 13). On the dip lines a low-angle thrust (1) cuts up as high as horizon B, about 200 ms below the sea floor (Fig. 12). Approaching the saddle area the fault abruptly steepens up and shows a normal component of displacement. At depth there is partitioning between the high angle fault with its oblique-slip normal sense of displacement and some lower-angle faults to the north of the fault, which display reverse senses of motion. A number of minor normal faults lie at the anticlinal crest, they die out vertically downwards within 500 ms time-depth from the sea floor and to the northeast. However, the oblique fault trend crosscuts the entire one second of data, which is completely atypical of the shallow normal faults. The 3D seismic data also shows a clear progressive steeping of the thrust into the oblique fault zone (Figs. 12 and 13). Consequently the oblique trend is not regarded as simply being caused by a shallow gravity-driven fault, but represents linkage of a normal fault with a deeper fault.

The strike-lines (Fig. 13) show a similar pattern to the dip lines. Passing to the SE, the thrust becomes high angle, with an apparent dip to the SW, plus the fault links with one or more of the shallow normal faults and curves back on itself. The southern-most section is notable because the oblique fault is steeply inclined, with a high apparent dip to the NE, and a normal sense of displacement. A symmetric pair of possibly oblique-slip normal faults converges towards the oblique fault at depth to form a small down-faulted graben at the surface.

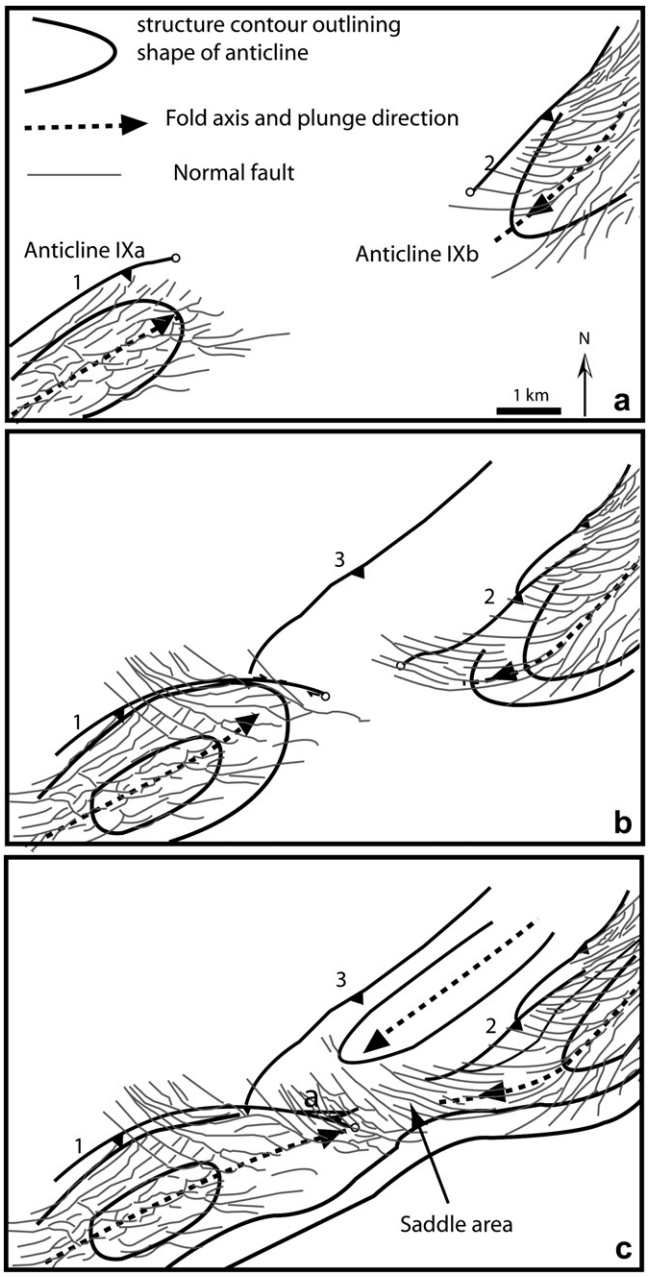

Fig. 15. Evolution of the oblique fault system affecting anticline IX. a, b) Early stages where the thrusts 1 and 2 are separated and have begun to propagate towards each other, c) Present-day stage where the anticlines associated with thrusts 1 and 2 have linked by lateral propagation, since the folds and faults lay en echelon the saddle zone (linkage zone between the two anticlines) forms an oblique feature.

8. Kinematics of the oblique fault zone

The transition to a normal fault-dominated fault system near the SE tip of the oblique fault would not be predicted for a simple oblique ramp system (Fig. 14b and c), both in terms of the change in dip direction, and sense of motion. An extensional or transtensional graben lies at the SE tip of the oblique fault. One further difference with a simple oblique ramp transfer zone is that anticline trends and terminations should show a geometric relationship with the oblique ramp (Fig. 14c). However, such a relationship is not apparent for anticline IX, the dip lines show that the fault changes position from the forelimb of the fold (where it is a thrust) to the core of the fold where it is a high angle oblique-slip fault (Fig. 14a and b).

Assuming that the highly oblique normal faults represent stages where a strongly plunging fold with surface topography was present, then the cross-cutting relationships between fold axis parallel normal faults and highly oblique faults gives some indication as to how propagation of the plunging fold segment developed in the structure (Fig. 15; Morley, 2007b). Two stages of plunging fold development are interpreted, the first stage involved propagation of the fold to the NE with time (Fig. 15a and b). In particular the presence of NNW–SSE trending normal faults near the fold crest suggest an early location of the plunging fold nose (Fig. 15b). The second stage occurred when the folds met, and began to merge in the saddle area. During this stage the oblique fault trend (a) developed across the elongated fold nose, close to, but not within the saddle area (Figs. 14 and 15c). The scenario for fault-fold development of anticline IX fits the model presented in Fig. 11c of Wilkerson et al. (2002) where fold development proceeds by the along-strike amalgamation of several small faults and associated folds.

9. Discussion

Fault systems at a high angle to the regional trend of thrusts are commonly explained as either conjugate systems of strike-slip faults or lateral and oblique ramps. However, the example from anticline IX shows a more complex oblique fault geometry that passes from a low angle, southeast-dipping thrust, to a high angle south-dipping thrust fault, then through a vertical segment, to an eastern segment that dips north and has a normal offset. To the east the fault dies out in a graben. The fault system lies within a linkage zone where two anticlines, slightly en echelon to each other, are in the process of merging.

Anticline IX is affected by numerous minor normal faults in the vicinity of the oblique fault that die out in the upper 500 m of section, (Figs. 12 and 13). The shallow normal faults swing around from lying parallel to the fold forelimb to a NW–SE trend at the plunging fold nose and are interpreted in response to the local relief created by fold geometry (Figs. 2 and 7). These crestal normal faults are restricted in occurrence to the anticlines, are oriented subparallel to the strike of the fold-controlled slope, and are most numerous on the steepest slopes (Morley, 2007b). Other NW–SE trending normal fault zones are apparent in Fig. 2 and they too are associated with surface dips displaying a gentle NE plunge. Consequently the normal faults are interpreted as gravity-driven. Stress perturbations appear to be a common feature of oblique faults, as modelled by Wilkerson et al. (1992). Out of plane strains associated with oblique faults in Wyoming, have been described where strike-slip faults and normal faults were locally generated (Apotria, 1995). While such stress perturbations probably play a role at depth in the oblique fault zone described, the shallow, gravity-driven normal faults in anticline IXa are an additional complexity.

The folds and thrusts in a deepwater setting are developed in poorly lithified, water-rich, commonly fine-grained sediments that tend to be strongly overpressured. These characteristics give fold and thrust geometries characteristics that depart from classic fault-bend folds (Suppe et al., 2004; Hesse et al., 2008; Franke et al., 2008). The oblique fault zone affecting anticline IX is associated with a young, growing fault and may later evolve into an oblique ramp if kinematic linkage occurs between the two thrusts (Fig. 14). Consequently the stage seen today is where the oblique zone is an oblique termination to a thrust (thrust 1), not a transfer zone between thrusts. Only later, if fault 2 links with the oblique fault zone can a true transfer zone develop (Fig. 14a). Such a kinematic

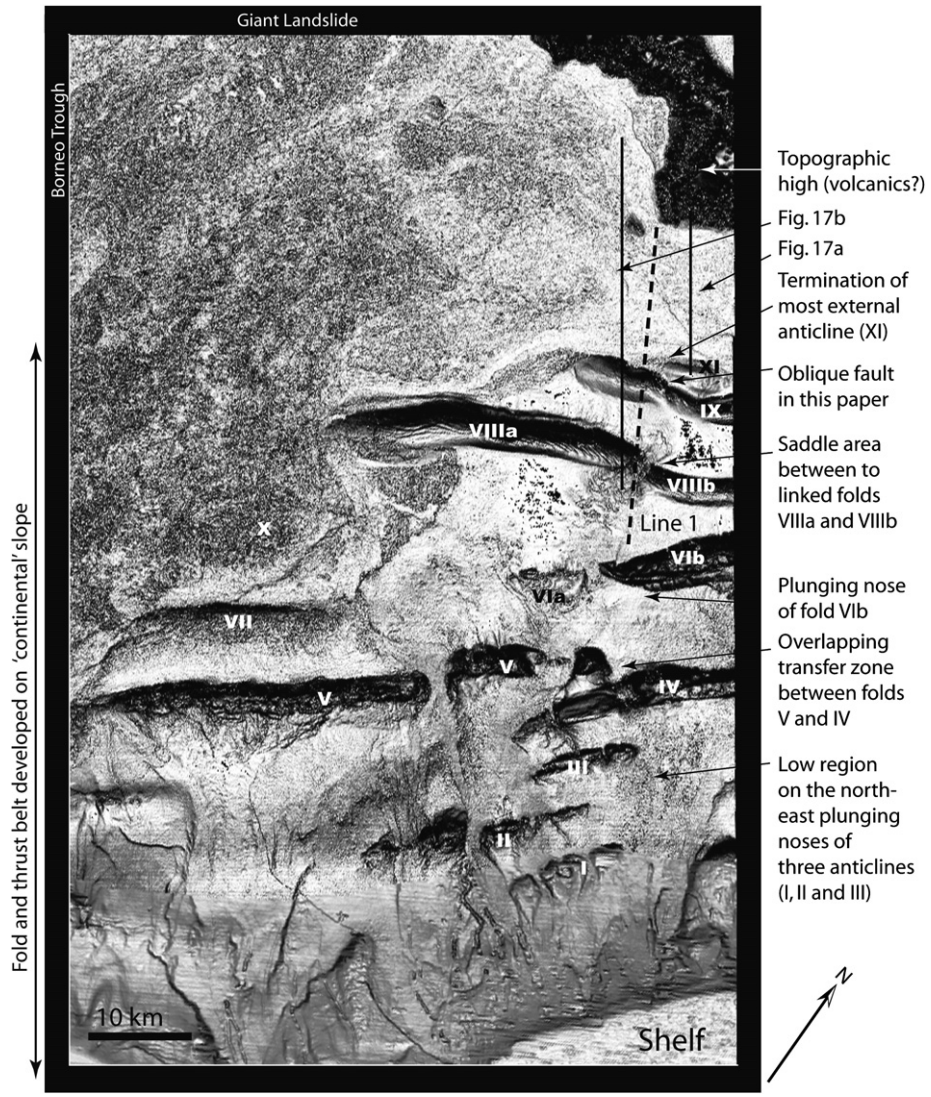

Fig. 16. Edge map of the water bottom reflection mapped from 3D seismic reflection data, for the outer shelf and slope region of offshore Brunei Darussalam (the sea floor morphology shown here has also been modified from Morley, 2009). See Fig. 1 for location.

linkage would either involve creation of a new fault segment through the region of the normal faults, or reactivation and inversion of the normal faults. The oblique fault zone does not appear to have originated as a feature inherent to the basal detachment. Indeed many of the thrust ramps probably originated as small faults growing within the sedimentary section that propagated downwards to meet the basal detachment during fold development (e.g. Eisenstadt and De Paor, 1987; Figs. 8 and 9a and c). Rather than a well defined thrust-oblique fault system propagating up from a basal detachment, the faults in this study probably developed from amalgamation of a number of faults scattered within the section that had begun to fold, over a broad zone undergoing simple shear (Fig. 8). Only as shortening increases may the detachment horizon become more discrete, and faults in the overlying section propagate downwards to meet the detachment. Similarly the oblique fault trend represents an amalgamation of faults (deeper oblique fault or faults that linked with shallower extensional faults, and laterally with thrust faults).

As described in Section 4.2 there are two sets of fold orientation (ENE–WSW and NE–SW) in the deepwater area (Fig. 10), which can be related to depositional patterns associated with the Baram and Champion deltas, and to folding and uplift patterns in the zones 1 and 2 structural provinces (Fig. 10). These features are likely to have caused the development of some oblique structures in the deepwater fold and thrust belt, particularly the area of the more proximal folds. In addition to the influence from the shelf on oblique structure development in the deepwater fold and thrust belt, there is a topographic feature on the seawards side that may also have been significant for anticline IX. This uplifted zone within the Dangerous Grounds crust lies about 14 km beyond the thrust front and probably represents a volcanic edifice, or a fault-bounded block. Whatever the origin, this uplifted region rises abruptly through the weaker Miocene–Holocene sediments of the Borneo Trough. The prominent NW–SE margin of the uplifted zone (Fig. 17) lines up with the oblique zone described in the paper (Fig. 16). Indentation of the topographic high into the sediments during underthrusting of the Dangerous Grounds crust beneath the sediments of the Baram Deltaic Province would have induced more shortening adjacent to the high NE of line 1 (Fig. 16). The formation of oblique structures would have helped accommodate the resulting lateral change in shortening.

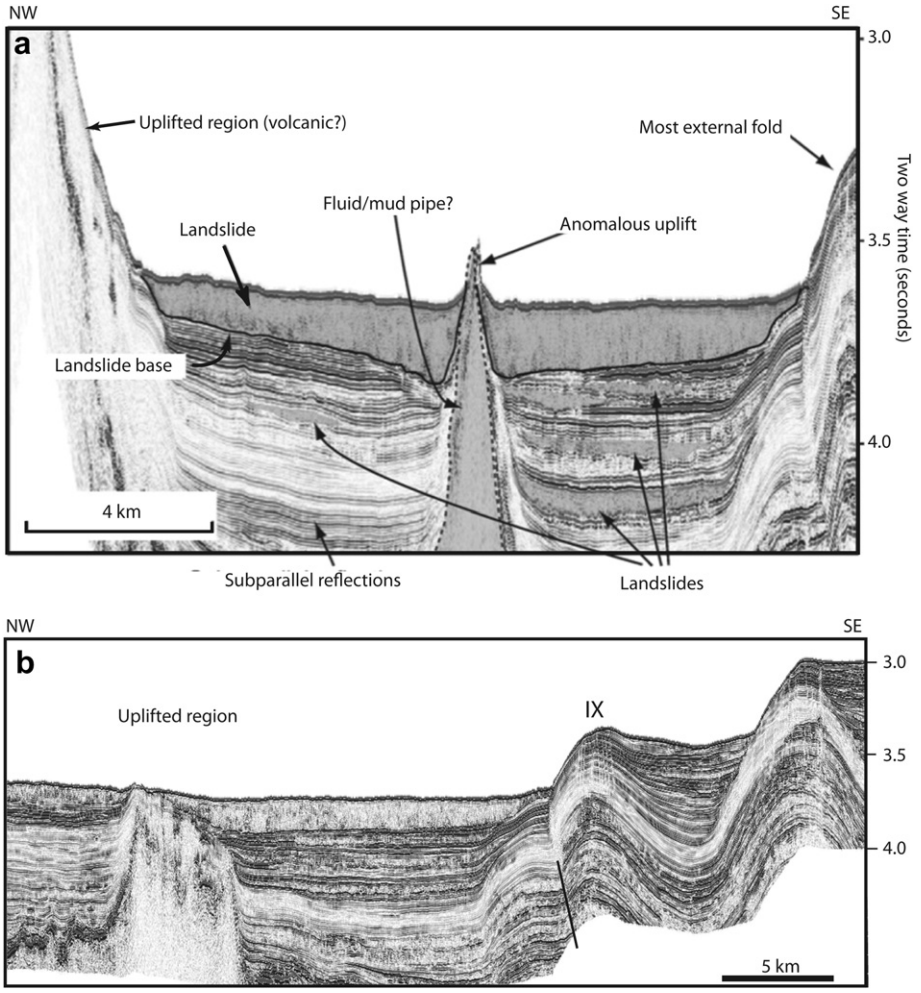

Fig. 17. Seismic lines running from the deepwater topographic high to the front of the deepwater fold and thrust belt, a) line immediately SW of the topographic high, b) line running up to the topographic high (Gee et al., 2007), see Fig. 16 for location.

10. Conclusions

The early stage of oblique fault development is shown on the NE plunging nose of anticline IX. The oblique zone appears to have originated as a response to a topographic high that indented the deepwater fold and thrust belt north of line 1 (Fig. 16). The oblique fault probably began to develop during the last 2.8–1.6 Ma, during which time the NE–SW trending anticline IX developed by the joining of two separate folds (IXa and IXb) in a saddle area. Passing along the oblique fault from the forelimb to backlimb the fault steepens up from a low-angle thrust, to sub-vertical dips, a component of extensional dip-slip offset is observed, and the fault terminates in an extensional graben. The deformation style along the oblique fault indicates 3D strain and complex stress patterns developed in the vicinity of the oblique fault. Presently the oblique fault zone has yet to be linked with a thrust fault passing to the NE, so it is not yet acting as a classic oblique ramp transfer zone. The oblique fault zone appears to be an amalgamation of several different faults that originated as deeper-seated thrusts, oblique-slip faults and shallow gravity-driven normal faults. While classic oblique ramps originate by propagation upward from the master detachment, it is suggested that following observed fault patterns in the deepwater setting that the oblique fault (and frontal thrusts) originated independently from the underlying detachment.

References

Apotria, T.G., 1995. Thrust sheet rotation and out-of-plane strains associated with oblique ramps: an example from the Wyoming salient, USA. Journal of Structural Geology 17, 647–662.

Apotria, T.G., Snedden, W.T., Spang, J.H., Wiltchko, D.V., 1992. Kinematic models of deformation at an oblique ramp. In: McClay, K.R. (Ed.), Thrust Tectonics. Chapman and Hall, pp. 141–154.

Brown, A.R., 1996. Interpretation of three-dimensional seismic data, fourth ed. American Association of Petroleum Geologists Memoir 42, p. 423.

Castonguay, S., Price, R.A., 1995. Tectonic heredity and tectonic wedging along an oblique hanging-wall ramp: the southern termination of the Misty thrust sheet, southern Canadian Rocky Mountains. Geological Society of America Bulletin 107, 1304–1316.

Corredor, F., Shaw, J.H., Bilotti, F., 2005. Structural styles in the deep-water fold and thrust belts of the Niger delta. AAPG Bulletin 89, 735–780.

Couzens, B.A., Dunne, W.M., 1994. Displacement transfer at thrust terminations: saltville thrust and sinking creek anticline, Virginia. Journal of Structural Geology 5, 383–395.

Dahlstrom, C.D.A., 1970. Structural geology in the eastern margin of the Canadian Rocky Mountains. Bulletin of Canadian Petroleum Geology 18, 332–406.

de Vera, J., Granado, P., McClay, K., 2009. Structural evolution of the orange basin gravity-driven system, offshore Namibia. Marine and Petroleum Geology. doi:10.1016/j.marpetgeo.2009.02.003.

Dubey, A.K., 1997. Simultaneous development of noncylindrical folds: frontal ramps, and transfer faults in a compressional regime: experimental investigations of Himalayan examples. Tectonics 16, 336–346.

Eisenstadt, G., De Paor, D.G., 1987. Alternative model of thrust-fault propagation. Geology 15, 630–633.

Fermor, P., 1999. Aspects of the three-dimensional structure of the Alberta foothills and front ranges. Geological Society of America Bulletin 111, 311–346.

Fischer, M.P., Woodward, N.B., Mitchell, M.M., 1992. The kinematics of break-thrust folds. Journal of Structural Geology 14, 451–460.
Franke, D., Barckhausen, U., Heyde, I., Tingay, M., Ramli, N., 2008. Seismic images of a collision zone offshore NW Sabah/Borneo. Marine and Petroleum Geology 25, 606–624.
Gee, M.J.R., Gawthorpe, R.L., Friedmann, S.J., 2005. Giant striations at the base of a submarine landslide. Marine Geology 214, 287–294.
Gee, M.J.R., Uy, H.S., Warren, J., Morley, C.K., Lambiase, J.J., 2007. The Brunei slide: a giant submarine landslide on the North West Borneo margin revealed by 3D seismic data. Marine Geology 246, 9–23.
Goldburg, B.L., 1984. Displacement transfer between thrust faults near the Sun River in the Sawtooth range, northwestern Montana. In: Montana Geological Society 1984, Field Conference, pp. 211–220.
Hall, R., 1996. Reconstructing Cenzoic SE Asia. In: Hall, R., Blundell, D.J. (Eds.), Tectonic Evolution of SE Asia. Geological Society of London Special Publication, vol. 106, pp. 153–184.
Hall, R., 2002. Cenozoic geological and plate tectonic evolution of SE Asia and the SW Pacific: computer-based reconstructions, model and animations. Journal of Asian Earth Sciences 20, 353–434.
Hall, R., Morley, C.K., 2004. Sundaland basins. In: Clift, P., Wang, P., Kuhnt, W., Hayes, D. (Eds.), Continental–Ocean Interactions within East Asian Marginal Seas. AGU Special Publication, vol. 149, pp. 55–87.
Hall, R., Nichols, G.J., 2002. Cenozoic sedimentation and tectonics in Borneo: climatic influences on orogenesis. In: Jones, S.J., Frostick, L. (Eds.), Sediment Flux to Basins, Causes, Controls and Consequences. Geological Society of London Special Publication, vol. 191, pp. 5–22.
Hazebroek, H.P., Tan, D.N.K., 1993. Tertiary tectonic evolution of the NW Sabah continental margin. Geological Society of Malaysia Bulletin 33, 195–210.
Hesse, S., Back, S., Franke, D., 2008. The deepwater fold-thrust belt offshore NW Borneo: gravity-driven versus basement-driven shortening. Geological Society of America Bulletin 121, 939–953.
Hinz, K., Schluter, H.U., 1985. Geology of the dangerous grounds, South China Sea and the continental margin off southwest Palawan. Results of SONNE cruises SO-23 and SO-27. Energy 10, 282–288.
Hinz, K., Fritsch, J., Kempter, E.H.K., Mohammad, A.M., Meyer, J., Mohamed, D., Vosberg, H., Weber, J., Benavidez, J., 1989. Thrust tectonics along the north-western continental margin of Sabah/Borneo. Geologische Rundschau 78, 705–730.
Holl, J.E., Anastasio, D.J., 1995. Kinematics around a large-scale oblique ramp, southern Pyrenees, Spain. Tectonics 14, 1368–1379.
Hutchison, C.H., Bergman, S.C., Swauger, D.A., Graves, J.E., 2000. A Miocene collisional belt in north Borneo: uplift mechanism and isostatic adjustment qualified by thermochronology. Journal of the Geological Society of London 157, 783–794.
Ingram, G.M., Chisholm, T.J., Grant, C.J., Hedlund, C.A., Stuart-Smith, P., Teasdale, J., 2004. Deepwater North West Borneo: hydrocarbon accumulation in an active fold and thrust belt. Marine and Petroleum Geology 21, 879–887.
James, D.M.D., 1984. The Geology and Hydrocarbon Resources of Negara Brunei Darussalam. Special Publication. Muzium Brunei and Brunei Shell Petroleum Company, Berhad, 164 pp.
King, R.C., Hillis, R.R., Tingay, M.R.P., Morley, C.K., 2009. Present-day stress and neotectonic provinces of the Baram delta and deep-water fold-thrust belt. Journal of the Geological Society of London 166, 1–4.
King, R., Backé, G., Morley, C.K., Hillis, R., Tingay, M. Balancing deformation in NW Borneo: quantifying plate-scale vs gravitational tectonics in a delta and deep-water fold-thrust belt system. Marine and Petroleum Geology, in press.
Lambiase, J.J., Tzong, T.Y., William, A.G., Bidgood, M.D., Brenac, P., Cullen, A.B., 2007. The West Crocker formation of northwest Borneo: a paleogene accretionary prism. Geological Society of America Special Paper 463, 171–184.
Levell, B.K., 1987. The nature and significance of regional unconformities in the hydrocarbon-bearing Neogene sequences offshore West Sabah. Geological Society of Malaysia Bulletin 21, 55–90.
Morgan, J.K., Karig, D.E., 1995. Kinematics and a balanced and restored cross-section across the toe of the eastern Nankai accretionary prism. Journal of Structural Geology 17, 31–45.
Morley, C.K., 1994. Fold-generated imbricates: examples from the Caledonides of southern Norway. Journal of Structural Geology 16, 619–631.
Morley, C.K., 2007a. Interaction between critical wedge geometry and sediment supply in a deepwater fold belt, NW Borneo. Geology 35, 139–142.
Morley, C.K., 2007b. Development of crestal normal faults associated with deep-water fold growth. Journal of Structural Geology 29, 1148–1163.
Morley, C.K., 2009. Growth of folds in a deep-water setting. Geosphere 5, 59–89.
Morley, C.K., Back, S., 2008. Estimating hinterland exhumation from late orogenic basin volume, NW Borneo. Journal of the Geological Society of London 165, 353–366.
Morley, C.K., Leong, L.C., 2008. Evolution of deep-water synkinematic sedimentation in a piggyback basin, determined from three-dimensional seismic data. Geosphere 4, 939–962.
Morley, C.K., Back, S., Crevello, P., Van Rensbergen, P., Lambiase, J.J., 2003. Characteristics of repeated, detached, Miocene–Pliocene tectonic inversion events, in a large delta province on an active margin, Brunei Darussalam, Borneo. Journal of Structural Geology 25, 1147–1169.
Morley, C.K., Tingay, M., Hillis, R., King, R., 2008. Relationship between structural style, overpressures, and modern stress, Baram delta province, northwest Borneo. Journal of Geophysical Research 113. doi:10.1029/2007JB005324.
Petronas, 1999. The Petroleum Geology and Resources of Malaysia. Petronas (Petroleum Nasional Berhad), Kuala Lumpur, Malaysia, 665 pp.
Pin, Y., Hailing, L., 2004. Tectonic-stratigraphic division and blind fold structures in Nansha waters, South China Sea. Journal of Asian Earth Sciences 24, 337–348.
Rich, J.L., 1934. Mechanics of low-angle overthrust faulting as illustrated by Cumberland thrust block, Virginia, Kentucky and Tennessee. AAPG Bulletin 18. doi:10.1036/3D932C94-16B1-11D7-8645000102C1865D.
Rowan, M.G., Linares, R., 2000. Fold-evolution matrices and axial surface analysis of fault bend folds: application to the Medina Anticline, Eastern Cordillera, Colombia. AAPG Bulletin 84, 741–764.
Sandal, S.T., 1996. The Geology and Hydrocarbon Resources of Negara Brunei Darussalam, (1996 Revision). Brunei Shell Petroleum Company/Brunei Museum, Syabas Bandar Seri Begawan, Brunei Darussalam, 243 pp.
Schreurs, G., Hanni, R., Vock, P., 2002. Analogue modelling of transfer zones in fold and thrust belts: 4-D analysis. Journal of the Virtual Explorer 7, 43–50.
Schluter, H.U., Hinz, K., Block, M., 1996. Tectono-stratigraphic terranes and detachment faulting of the South China Sea and Sulu Sea. Marine Geology 130, 39–78.
Simmons, W.J.F., Socquet, A., Vigny, C., Ambrosius, B.A.C., Haji Abu, S., Promthon, C., Subarya, C., Sarsito, D.A., Matheussen, S., Morgan, P., Spakman, W., 2007. A decade of GPS in Southeast Asia: resolving Sundaland motion and boundaries. Journal of Geophysical Research 112, B06420. doi:10.1029/2005JB003868.
Soto, R., Casas, A.M., Storti, F., Faccenna, C., 2002. Role of lateral thickness variations on the development of oblique structures at the western end of the Southern Pyrenean Central Unit. Tectonophysics 350, 215–235.
Suppe, J., 1983. Geometry and kinematics of fault-bend folding. American Journal of Science 283, 684–721.
Suppe, J., Medwedeff, D.A., 1984. Geometry and kinematics of fault-propagation folding. Journal of Geophysical Research 89, 87–101.
Suppe, J., Connors, C.D., Zhang, Y., 2004. Shear fault-bend folding. In: Mc Clay, K.R. (Ed.), Thrust Tectonics and Hydrocarbon Systems. AAPG Memoir, vol. 82, pp. 303–323.
Tingay, M.R.P., Hillis, R.R., Morley, C.K., Swarbrick, R.E., Drake, S.J., 2005. Present day stress orientations in Brunei: a snapshot of prograding tectonics in a Tertiary delta. Journal of the Geological Society of London 162, 39–49.
Wilkerson, S.M., Marshak, S., Bosworth, W., 1992. Computerized tomographic analysis of displacement trajectories and three-dimensional fold geometry above oblique thrust ramps. Geology 20, 439–442.
Wilkerson, S.M., Apotria, T., Farid, T., 2002. Interpreting the geologic map expression of contractional fault-related fold terminations: lateral/oblique ramps versus displacement gradients. Journal of Structural Geology 24, 593–607.